A review of the coefficient of thermal expansion and thermal conductivity of graphite

ZHAO Lu[1], TANG Jiang[2,3], ZHOU Min[2,3], SHEN Ke[2,3,*]

(1. *Tsinghua-Berkeley Shenzhen Institute*, *Tsinghua University*, *Shenzhen* 518055, *China*;
2. *College of Materials Science and Engineering*, *Hunan University*, *Changsha* 410082, *China*;
3. *Hunan Province Key Laboratory for Advanced Carbon Materials and Applied Technology*, *Hunan University*, *Changsha* 410082, *China*)

Abstract: Graphite serves as a key material for heat dissipation in electronic devices and nuclear engineering due to its remarkable thermal properties. The thermal expansion and conductivity of graphite have always been major scientific parameters in the field of carbon materials. Therefore, theoretical and experimental research in this area has received extensive attention. Research progress on the thermal expansion coefficient and thermal conductivity of graphite crystals is reviewed. Theoretical and experiment results on the thermal expansion coefficient of graphite are first introduced, followed by a discussion of the methods for measuring graphite thermal conductivity and the special phonon scattering mechanism in graphite. Finally, the uses of graphite in thermal management are summarized, and the development prospects in this field are discussed.

Key words: Graphite; Thermal expansion; Thermal conductivity; Thermal management

1 Introduction

Graphite is an excellent thermal-management material that plays a key role in the fields of electronics, aerospace, and nuclear engineering owing to its unique thermal properties. For example, with the rapid increase in the power density of modern electronics, heat dissipation has become a bottleneck in the operational efficiency, service lifetime, and user safety of devices. In addition, the thermal expansion behavior of graphite materials must be considered in the engineering design employed over a wide temperature range[1–3]. Therefore, it is necessary to fully understand the thermal conductivity and thermal expansion behavior of graphite.

Graphite is an allotrope of carbon composed of a series of hexagonal network carbon atoms, as shown in Fig. 1[4]. Within each basal plane, the carbon atoms were sp^2 hybridized and bound to each other by covalent bonds. The interactions between different basal planes are weak van der Waals forces. Therefore, the layered structure of graphite results in highly anisotropic properties. In general, the in-plane direction is called the "a-direction," and the out-of-plane direction is called the "c-direction."

Thermal expansion is a fundamental property of a material and is an important characteristic for preventing thermal cracks at the interface of heterogeneous composites. For graphite, the negative coefficient of thermal expansion (CTE) has been recognized and intensively studied. Furthermore, graphite is a structural material in nuclear engineering, and understanding its CTE is extremely important during the design of a reactor. It is necessary for predicting the thermal expansion behavior of nuclear graphite in a reactor environment.

A thorough understanding of thermal transport in graphite is of significance in fundamental science and applications. Recently, progress in thermal measurements has facilitated the experimental study of micro/nanoscale thermal transport. As representative two-dimensional materials, graphite and graphene are excellent platforms for studying phonon scattering in such unique systems, such as ballistic phonon transport[5], hydrodynamic phonon transport (second sound)[6,7], and four-phonon scattering[8,9].

Research on the thermal conductivity of graphite has significantly improved its applications in the field

Received date: 2021-08-11; **Revised date:** 2022-01-24
Corresponding author: SHEN Ke, Professor. E-mail: shenk@hnu.edu.cn
Author introduction: ZHAO Lu, Ph.D candidate. E-mail: zhaolou17@mails.tsinghua.edu.cn

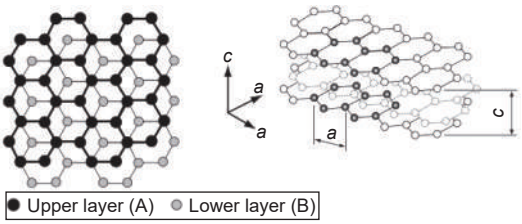

Fig. 1　Schematic diagram of graphite structure[4]. Reprinted with permission.

of thermal management. Graphite-based materials, including highly conductive graphite thin films and thermal interface composite materials, play an important role in the heat dissipation of electronic devices.

In this paper, the theory and experimental determinations of graphite CTE and thermal conductivity are reviewed. The aim is not only to clarify the current understanding of graphite but also to provide guidance for future research on more sophisticated factors that affect the thermal expansion and heat-spreading behavior of graphite.

2　Theory of thermal expansion of graphite

The theory of thermal expansion of graphite was first developed by Riley[10] during the 1940s. The heat capacity at a constant volume, C_v for a hexagonal crystal such as graphite can be considered to be composed of two components, C_{v_x} and C_{v_z}

$$C_v = \frac{2}{3}C_{v_x} + \frac{1}{3}C_{v_z} \tag{1}$$

Where these two components refer to vibrations perpendicular and parallel to the hexagonal axis, and are expressed by the Debye functions as follows:

$$C_{v_x} = 3RD\left(\frac{\Theta_x}{T}\right);\ C_{v_z} = 3RD\left(\frac{\Theta_z}{T}\right) \tag{2}$$

where Θ_x and Θ_z are the Debye temperatures associated with in-plane and out-of-plane lattice vibrations, respectively.

Using the experimentally measured C_p, the corresponding derived values for C_v, Θ_x, and Θ_z were determined to be

$$\Theta_x = 2280;\ \Theta_x = 760$$

Based on these assumptions, the final form of the expressions for the two expansion coefficients can be written as follows:

$$\alpha_a = AC_{v_a} + BC_{v_c} + CT \tag{3}$$

$$\alpha_c = LC_{v_a} + MC_{v_c} + NT \tag{4}$$

where α_a and α_c are the thermal expansion coefficients of graphite in and out of the plane, respectively; T is the temperature; and A, B, C, L, M and N are treated as constants.

At extremely high temperatures, the Debye function approaches unity. For graphite, this condition is reached when T is greater than 2 000 K. Above this temperature, $C_v \approx C_{v_a} \approx C_{v_c} \approx 3R$, where R is the gas constant. Hence, the expansion coefficient can be approximated as a linear function of T:

$$\alpha_a = (A + B)3R + CT. \tag{5}$$

In this case, if C is negligible, α_a is approximately constant at an extremely high temperature and has a value of $(A + B)3R$. By fitting the experiment values, Riley obtained the values of A, B, C, L, M, and N listed in Table 1. The resulting theoretical plots of α_a and α_c are shown in Fig. 2a and 2b, respectively.

In Fig. 2a, the theoretical curve gives that the value of α_a is equal to 0 at the temperature of 383 °C, where the in-plane thermal expansion coefficient of graphite changes from negative to positive. This indicates that the in-plane size of graphite first decreases and then increases within this temperature range. The negative basal CTE of graphite is attributed to the Poisson contraction of the basal planes associated with the large expansion in the c-axis. The value of $(A + B)3R$ was calculated as approximately 1.5×10^{-6} K^{-1} according to Riley's fitting results.

The theoretical curve of α closely agrees with the experiment values (Fig. 2b). The step-like characteristics of this curve are of particular interest. Furthermore, α_c increased rapidly within the temperature

Table 1　Various results for coefficients in α_a and α_c.

		A (J mol^{-1})	B (J mol^{-1})	C (deg^{-2})	L (J mol^{-1})	M (J mol^{-1})	N (deg^{-2})
1945	Riley	1.620×10^{-7}	-1.013×10^{-7}	0	-7.70×10^{-7}	1.38×10^{-6}	1.08×10^{-8}
1972	Morgan	1.677×10^{-7}	-1.036×10^{-7}	-8.3×10^{-11}	-7.93×10^{-7}	1.56×10^{-6}	7.19×10^{-9}
1964	Kellett and Richards	1.777×10^{-7}	-1.065×10^{-7}	0			
2005	Tsang				-5.05×10^{-7}	1.40×10^{-6}	5.15×10^{-9}

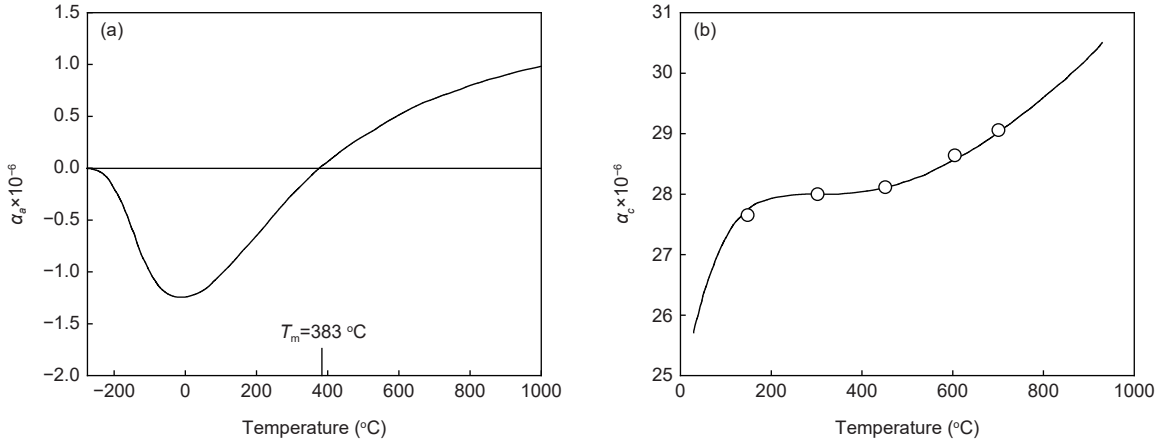

Fig. 2 (a) In-plane thermal expansion coefficients of graphite at different temperatures[10] and (b) Out-of-plane thermal expansion coefficient of graphite at different temperatures[10]. Reprinted with permission.

range from 0 °C to 127 °C.

Based on more experimental data from Steward et al.[11], Nelson and Riley[10], and Harrison[12], α_a and α_c are fitted using Riley's theory, shown in Fig. 3a and b, respectively. Morgan's fitting result[13] of α_a provides a closer estimation owing to the nonzero value for the temperature term (C). Morgan's fitting result also predicted that the value of α_a is equal to 0 at temperature of 393.6 °C. However, the estimation of α_c has certain drawbacks compared with the experiment data. The estimation from Riley[14] provides better agreement at low temperatures. However, the value of α_c is overestimated at high temperatures. Morgan's coefficients[13] provide a better estimation at high temperatures, although there is a hump in the profile at low temperatures, which is not present in the experiment data.

Tsang et al.[15] not only provided an excellent review of the graphite thermal expansion theory, but also proposed a method for calculating the CTE values over different temperature ranges.

Table 1 summarizes the values of the constants A, B, C, L, M and N in the thermal expansion coefficient expressions based on Riley's theory[14]. In general, the thermal expansion coefficients of graphite are highly anisotropic. At 300 K, the value of α_a is equal to -1.5×10^{-6} K^{-1}, and the value of α_c is equal to 27.0×10^{-6} K^{-1}[10].

In 2005, Mounet et al.[16] presented a full first-principles study of the thermodynamic properties of graphite using the Perdew–Burke–Ernzerhof generalized gradient approximation, including the thermal expansion behavior. The theoretical in-plane and out-of-plane thermal expansion coefficients of graphite within the temperature range from 0 to 2 500 K are shown in Fig. 4a and 4b, respectively. Although α_a was

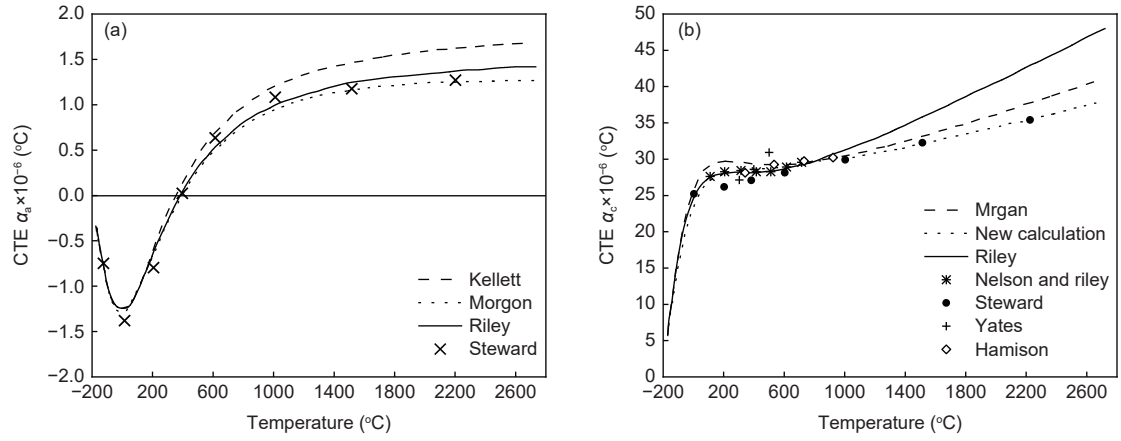

Fig. 3 (a) Plots of α_a against temperature compared with experiment results from Steward[15], (b) Plots of α_c against temperature compared with experiment results from Steward, Nelson and Riley, Yates and Harrison[15]. Reprinted with permission.

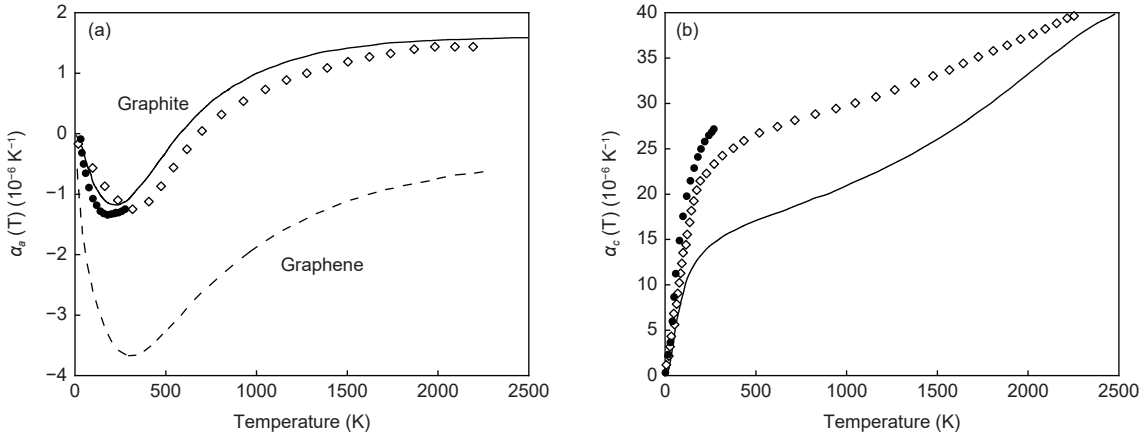

Fig. 4　(a) In-plane thermal expansion coefficient of graphite as a function of temperature for graphite (solid line) and graphene from *ab initio* study. The experiment data for graphite are marked by filled circles and open diamonds[16]. (b) Out-of-plane thermal expansion coefficient of graphite as a function of temperature for graphite (solid line) from *ab initio* study. The experiment data for graphite are marked by filled circles and open diamonds[16]. Reprinted with permission.

slightly overestimated in comparison with the experiment results, it agreed well overall, even at high temperatures. Moreover, α_a was confirmed to be negative from 0 to 600 K. This feature is absent in diamond but much more apparent in graphene, whose α_a remains negative at up to 2 300 K. For the out-of-plane case, αc holds well up to 150 K. However, α_c is underestimated by approximately 30% at 1 000 K.

3　Experimental determination of graphite thermal expansion coefficient

The experimental determination of the graphite CTE depends on the measurement of the dimensional change in the graphite crystal with temperature. The most convenient method of in situ X-ray diffraction (XRD) is employed to measure the change in the graphite lattice dimensions with temperature.

The anisotropic graphite lattice dimensions can be extracted based on Bragg's law as

$$2d\sin\theta = \lambda \tag{6}$$

where λ is the wavelength of the incident X-rays. With the change of temperature, the thermal expansion behavior of graphite led to the migration of diffraction peaks in the XRD patterns. The out-of-plane CTE (α_c) was obtained by checking the graphite interlayer spacing (d_{002}, d_{004}, ⋯), whereas the in-plane CTE (α_a) was obtained by observing the (100) reflection.

The linear thermal expansion coefficient, $\alpha(t)$, is given by $\alpha(t) = 1/l_0(\mathrm{d}l/\mathrm{d}t)$. In practice, $a(t)$ can be calculated as follows:

$$\alpha(t) = \frac{1}{l_0}\frac{(l_1 - l_2)}{(t_1 - t_2)} \tag{7}$$

where l_1 and l_2 are the lattice parameters at temperatures t_1 and t_2, respectively, and $t = (t_1+t_2)/2$. In general, there is a difference between the macroscopic length change with temperature measured optically or mechanically and the lattice parameter change measured through XRD. However, this difference is believed to be small and is neglected in the measurement of the CTE of graphite (Fig. 5).

For the out-of-plane CTE, Nelson and Riley[10] applied XRD at various temperatures, and the calculated apparent length of the unit cell was plotted against the extrapolation function $\frac{\cos^2\theta}{\sin\theta} + \frac{\cos^2\theta}{\theta}$ to ob-

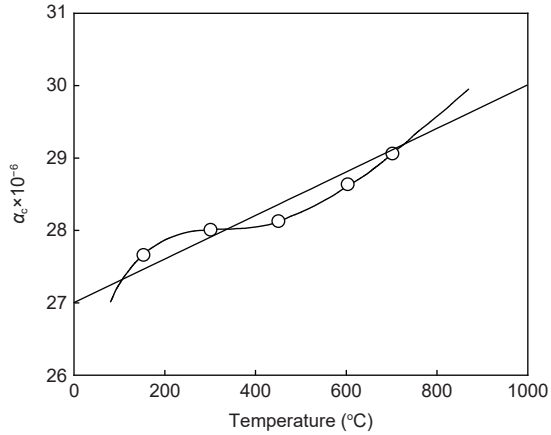

Fig. 5　Comparison of the observed α_a values with the best linear fitting with temperature[10]. Reprinted with permission.

tain the true lattice dimensions.

In situ XRD has been widely employed to measure the CTE of graphite. For example, Steward and Cook[11] measured the interlayer spacing d_{002} of natural graphite at room temperature, 728 °C and 1 188 °C. A recent *in situ* XRD study by Boi et al.[17] showed anomalous unit-cell c-axis shifts in highly oriented pyrolytic graphite (HOPG) measured at a magic angle.

For the in-plane CET, Kellett and Richards[18] used graphite specimens in rod form with dimensions of 10 mm × 2 mm × 1.5 mm, made from HOPG, which had been graphitized at 2 980 °C. The rods were cut in order to the basal planes parallel to the smaller (10 mm × 1.5 mm) sides. This enabled the maximum possible intensity to be obtained from the cross-lattice reflections using a larger side (10 mm × 2 mm) as the reflecting surface (Fig. 6).

The variation of the a-dimension of graphite in the temperature range of −196 °C to 3 000 °C is shown explicitly in Fig. 7a. The a-dimension of the single-crystal graphite showed a minimum between 350 °C and 400 °C, which is consistent with the results of Nelson and Riley[10] and the theory by Riley[14] . Using the experiment data in Fig. 10 over the temperature range from −196 to 3 000 °C, the fitting values for the constants A, B, and a_0 yielded a CTE curve as a function of temperature, as shown in Fig. 7b. This curve agreed with the theory predicted by Riley et al. In particular, the thermal expansion coefficient appears to be approaching a value of 1.2×10^{-6} °C^{-1} at extremely high temperatures.

The graphite domain size dependence of the thermal expansion of nanographite was investigated by Akikubo et al.[19] using *in situ* high-temperature XRD over the range from 25 to 500 °C, as shown in Fig. 8. Carbon nanowalls (CNWs) composed of nanographite domains were employed as the nanographite samples. CNWs with an appropriate domain size exhibit positive thermal expansion in the in-plane (a-axis) and out-of-plane (c-axis) directions, in contrast to highly ordered pyrolytic graphite (HOPG), which shows negative thermal expansion along the in-plane direction. The results confirmed that reducing the size of the graphite domain lowered the temperature at which thermal expansion along the in-plane direction changed from negative to positive. This switch to positive thermal expansion can be explained by the suppression of the out-of-plane vibration, which is related to the thermal contraction and is caused by the smaller domain of CNWs compared to HOPG.

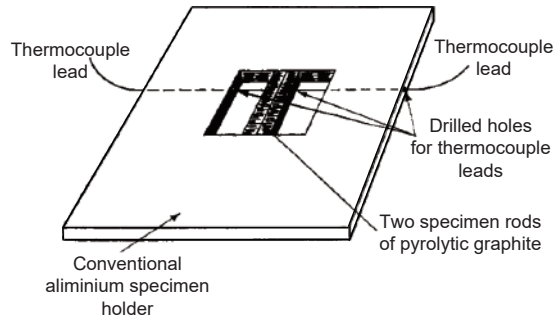

Fig. 6 Specimen and holder for low-temperature attachment for *in situ* XRD measurement[18]. Reprinted with permission.

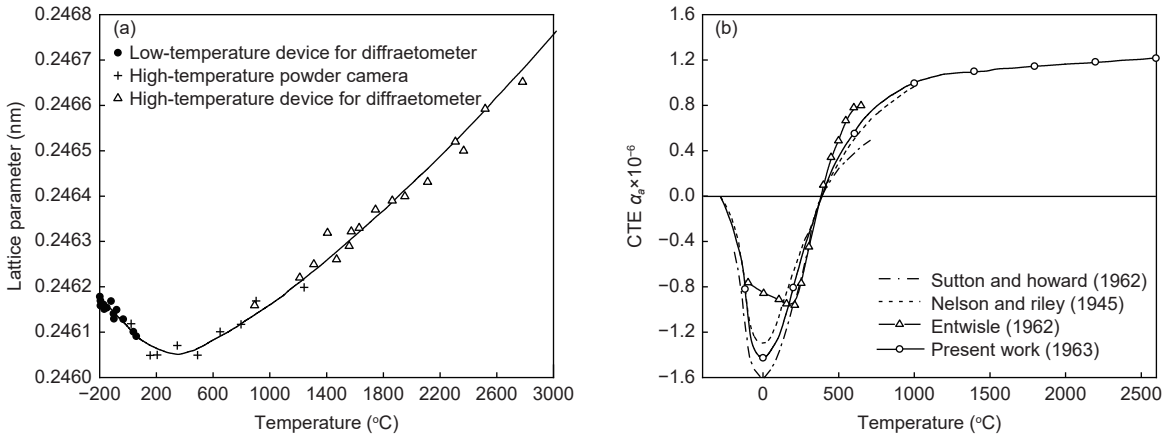

Fig. 7 (a) Plot of the variation of the a-dimension with temperature[18], (b) Plot of the variation of the coefficient of thermal of expansion perpendicular to the hexagonal axis with temperature: comparison with previous measurement[18]. Reprinted with permission.

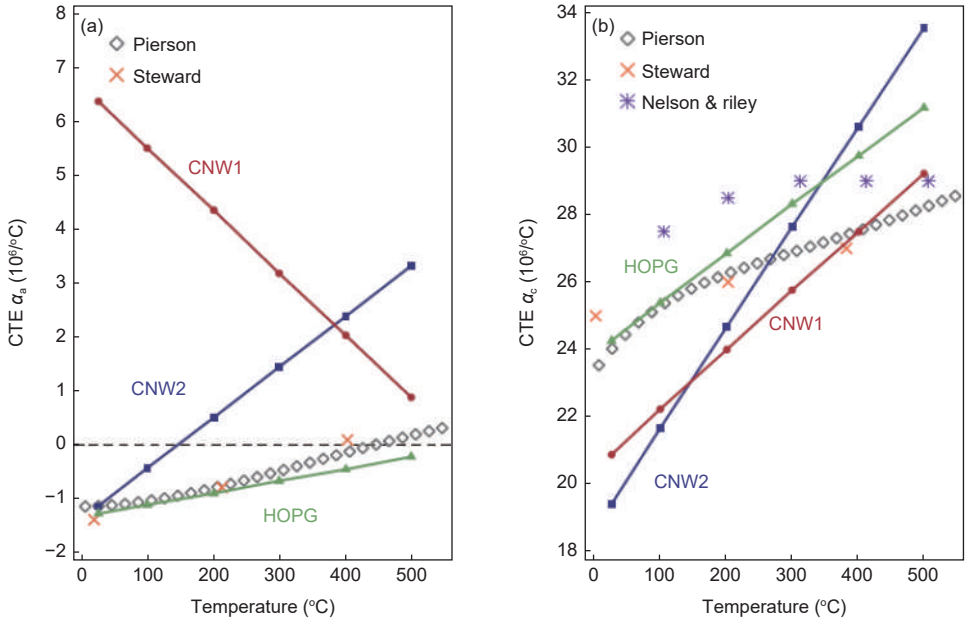

Fig. 8　Temperature dependences of the CTEs in the (a) a- and (b) c-directions of CNW1, CNW2 and HOPG[19]. Reprinted with permission.

The measurement of the c-axis thermal expansion coefficient of graphite using XRD involves a microscopic measurement method, whereas the interferometric measurement of the thermal expansion coefficient of graphite uses a macroscopic observation method. Interferometric measurements require a higher degree of grain orientation of the graphite sample because the interferometric method can only reflect the change in the thermal expansion coefficient through macroscopic size changes in a and c directions. As the basic principle of interferometry, as the temperature increases, the size L of the graphite sample in a specific direction changes, resulting in a change in the optical path difference of the two beams with a wavelength of λ reflected in a specific direction, leading to changes in the order N of the interference fringes. There is a quantitative relationship between the order of the interference fringes and the change in size of the graphite sample, $\Delta L = N\lambda/2$, from which the change in size of the graphite sample at different temperatures can be obtained. In 1970, Bailey and Yates[9] used interferometry to measure the thermal expansion coefficients of well-oriented pyrolytic graphite in the inner and outer directions of pyrolytic graphite within the temperature range of 30 to 270 K.

In 2016, Alexander et al.[20] reported a direct measurement of the instantaneous in-plane (ab-direction) CTE of free-standing single-crystal graphite using the thermal bulge method. Scotch tape was used to obtain 40-nm thick graphite flakes through the micromechanical cleavage of high-quality graphite flakes. The naturally bulged shape of the samples made it possible to easily measure the CTE (Fig. 9). The measured in-plane CTE was negative and gradually decreased from 1.8×10^{-6} to 0.7×10^{-6} °C^{-1} when the samples were heated from 25 to 225 °C, as shown in Fig. 9.

4　Thermal conductivity of graphite

4.1　Thermal conductivity of pyrolytic graphite

The accurate measurement of the thermal conductivity of graphite is the basis of its practical application and research on basic physical problems. Because the structure of pyrolytic graphite is closest to single-crystal graphite, several handbooks provide recommended values for the temperature-dependent thermal conductivity of graphite. The *CRC Handbook of Chemistry and Physics*[21] and Ho et al.[22] show that the in-plane thermal conductivity ($\Lambda_{//}$) and the cross-plane thermal conductivity ($\Lambda_{\perp}$) of pyrolytic graphite are 1 950-2 000 Wm^{-1}K^{-1} and 5.5-6 Wm^{-1}K^{-1} at 300 K, respectively. However, these two values at

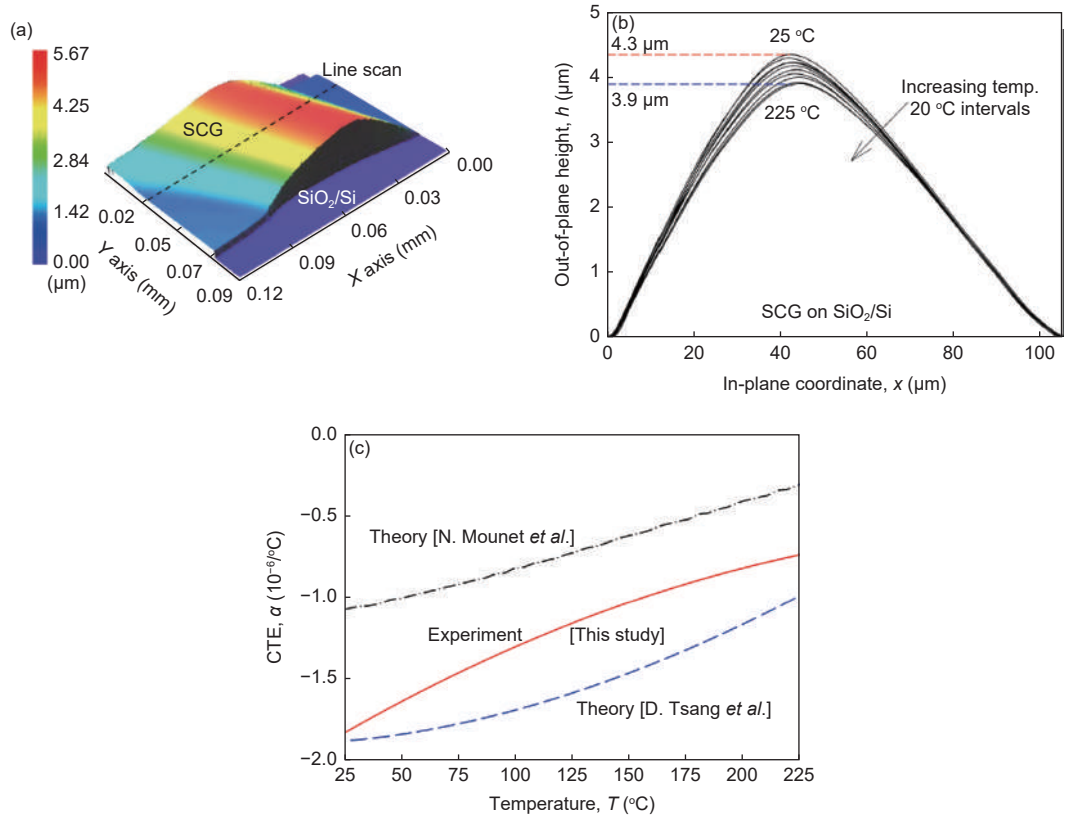

Fig. 9 (a) Typical topography of the graphite surface during heating, and (b) successive out-of-plane height profiles of a graphite crystal heated from 25 °C to 225 °C, scanned along the line indicated in (a). (c) Comparison of measured and theoretical CTEs for single-crystal graphite[20]. Reprinted with permission.

300 K are 2 000 and 9.5 $Wm^{-1}K^{-1}$, respectively, in the TPRC data[23]. Taylor et al.[24] and Nihira et al.[25] measured the thermal conductivity of HOPG using the steady-state method, and $\Lambda_{//}$ and $\Lambda_{\perp}$ were 1 500-1 700 $Wm^{-1}K^{-1}$ and 6-8 $Wm^{-1}K^{-1}$ at 300 K, respectively. As shown in Fig. 10, the thermal conductivity in both directions increased with decreasing temperature, and a peak occurred at approximately 80 K, indicating a shift from phonon–phonon scattering to phonon–boundary scattering.

With the progress in thermal measurement techniques, transient methods such as time-domain thermoreflectance (TDTR) and frequency-domain thermoreflectance (FDTR) have become powerful tools for investigating the anisotropic thermal properties of 2D materials such as graphite. Schmidt[26] measured the anisotropic thermal conductivity of HOPG by taking advantage of the fact that the sensitivities of the measurement parameters of laser spot size and frequency for $\Lambda_{//}$ and $\Lambda_{\perp}$ are different. The results were 1 875-2 034 $Wm^{-1}K^{-1}$ and 5.72 $Wm^{-1}K^{-1}$ for $\Lambda_{//}$ and $\Lambda_{\perp}$, respectively. Several modified techniques have been developed based on the TDTR. Feser et al.[27] developed a beam offset TDTR method and obtained results of 1 800-2 100 $Wm^{-1}K^{-1}$ for $\Lambda_{//}$ and 5.1-6.1 $Wm^{-1}K^{-1}$ for $\Lambda_{\perp}$ of graphite at 300 K. The variable spot-size method proposed by Jiang et al.[28] can measure the thermal conductivity of layered materials with strong anisotropy. Thus, $\Lambda_{//}$ and $\Lambda_{\perp}$ of graphite measured by the variable spot-size method were 1 900 ± 240 and 6.5 ± 0.7 $Wm^{-1}K^{-1}$ at 300 K, respectively. Qian et al.[29] utilized the FTDR method with no transducer, and the thermal conductivity of graphite at 300 K in these 2 directions was found to be 1 900 and 6.1 $Wm^{-1}K^{-1}$.

4.2 Thermal conductivity of graphite with defects

In addition to pyrolytic graphite, there are various types of graphite, such as natural graphite, hot-pressed graphite, chemical vapor deposition (CVD) graphite film, and polycrystalline graphite, in which different structural defects, functional groups, crystalline grain sizes, and orientations have impacts on the

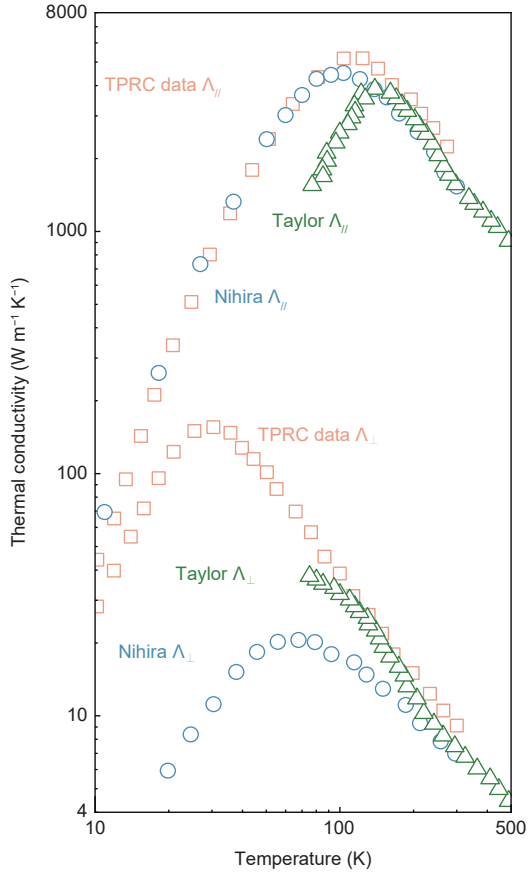

Fig. 10　Temperature-dependent thermal conductivity of graphite: Thermal conductivity in TPRC handbook data[23] (orange open squares) and previous reports by Taylor[24] (olive open triangle) and Nihira et al.[25] (blue open circles). Reprinted with permission.

thermal properties. Boundary scattering is the main source of phonon scattering in polycrystalline graphite, and the effective crystal conductivity is reduced through the combined porosity/tortuosity factor[30]. The interstitial and vacancy defects caused by neutron irradiation significantly affect the thermal properties of nuclear-grade polycrystalline graphite in nuclear reactors. The results show that neutron irradiation remarkably reduced the thermal conductivity of graphite[31,32], and a recovery of the thermal conductivity was observed after annealing. Although the thermal conductivities of pristine graphite of various grades are different, after the same dose of irradiation, the temperature dependence of their thermal conductivities is similar.

Despite being a type of polycrystalline graphite, hot-pressed graphite has a strongly preferred orientation and anisotropy in thermal conductivity, and can be used as a low-cost thermal management material. The thermal conductivities of a number of hot-pressed graphite blocks[33,34] approach 1 300-1 800 $Wm^{-1}K^{-1}$ and 5.5-10 $Wm^{-1}K^{-1}$ at 300 K in 2 orthogonal directions.

Dresselhaus et al.[35,36] studied the thermal conductivities of graphite intercalation compounds. It was found that both $\Lambda_{//}$ and $\Lambda_{\perp}$ were significantly suppressed because of the strong phonon-defect scattering. In addition, the contributions from electrons and phonons were investigated, and the temperature-dependent thermal conductivities of graphite–$FeCl_3$ acceptor intercalation compounds and stage-5 potassium donor compounds showed that the electron contribution dominated the thermal conductivity at low temperatures, whereas the lattice contribution was dominant at higher temperatures.

4.3　Thickness-dependent thermal conductivity of graphite

The thermal conductivity of graphite varies significantly from the bulk to a (quasi-) two-dimensional state. It is essential to study the effect of thickness on the thermal conductivity of graphite. The dominant mechanism of the in-plane thermal conductivity changes with increasing thickness. In Fig. 11a, from a single layer to a few layers, the experiment results show that the thermal conductivity decreases gradually with an increase in the number of layers. When it reaches four layers, $\Lambda_{//}$ of the suspended graphene is close to that of bulk graphite[37]. By contrast, the thermal conductivity of graphene on the substrate increases or remains unchanged with increasing layers[38–40], which differs from that of suspended graphene. This is mainly because the ZA phonon mode has a relatively large low-frequency state density in single-layer graphene. Therefore, its contribution from the ZA mode is relatively large and can reach approximately 70%[41]. With an increasing number of layers, interlayer coupling results in strong scattering of low-frequency phonons and a decrease in the thermal conductivity. The contribution of the ZA phonon mode is severely inhibited or even disappears in graphene on a substrate[40]. Therefore, the change in

the thermal conductivity with the thickness of graphene on the substrate is not intrinsic.

As the thickness continues to increase, boundary scattering limits the thermal conductivity. However, the thickness dependence should be verified through experiments and calculations.

A recent study reported the ultrahigh $\Lambda_{//}$ of 4 300 $Wm^{-1}K^{-1}$ for 8.5-μm thick graphite at room temperature, and $\Lambda_{//}$ decreased with the sample thickness, and $\Lambda_{//}$ of 580 μm thick sample was 650 $Wm^{-1}K^{-1}$[42]. The reduction in the thermal conductivity with increasing thickness was attributed to the phonon hydrodynamics phenomenon, and the ultrahigh thermal conductivity of the 8.5 μm thick sample was ascribed to the suppression of the Umklapp process in the thinned film. Another experiment conducted by Wang et al.[43] also showed that the thermal conductivity of graphite increased with a decrease in the thickness, and the value of 3 200 $Wm^{-1}K^{-1}$ was obtained in an 800-nm thick film. However, it is concluded that the thickness-dependent $\Lambda_{//}$ can be attributed to the sample quality. Commercial graphitized polyimide films also show a strong thickness dependence, with the thermal conductivity ranging from 700 to 1 950 $Wm^{-1}K^{-1}$ as the thickness decreases from 100 to 10 μm, which can be attributed to the molecular orientation of the polyimide[44]. Experiment and computational results on the thickness dependence of $\Lambda_{//}$ for graphite are still lacking.

In the cross-plane direction, the thickness dependence of $\Lambda_{\perp}$ is mainly caused by boundary scattering, which is often used to measure the phonon mean free path (MFP) along the c-axis.

4.4 Phonon mean free paths in graphite

The phonon MFP is a decisive factor in the thermal conductivity of a material. The comparison of the phonon MFP of phonons and the sample geometry determines the type of phonon transport, which is either diffusion or ballistic transport. In the in-plane direction, experiment and theoretical calculations show that the MFPs of both single-layer graphene and bulk graphite are greater than 10 μm[45]. In the cross-plane direction, the interlayer forces of graphite are van der Waals forces, which are much weaker than the in-plane interaction forces. Therefore, it was initially indicated by the simple kinetic theory that the cross-plane MFP was as short as a few nanometers[24]. However, a theoretical study in 2014[46] has shown that the commonly believed MFP is drastically underestimated. The cross-plane MFP of graphite has also been studied theoretically using a non-equilibrium molecular dynamics simulation[46]. The simulation results show that phonons with MFPs from 2-2 000 nm contribute approximately 80% of the graphite $\Lambda_{\perp}$, and phonons with MFPs larger than 100 nm contribute more than 40%. Harb et al.[47] measured $\Lambda_{\perp}$ of graphene with a thickness of 35 nm to be approximately 0.7 $Wm^{-1}K^{-1}$, which is an order of magnitude lower than that of bulk graphite. This phenomenon may have resulted from the previous underestimation

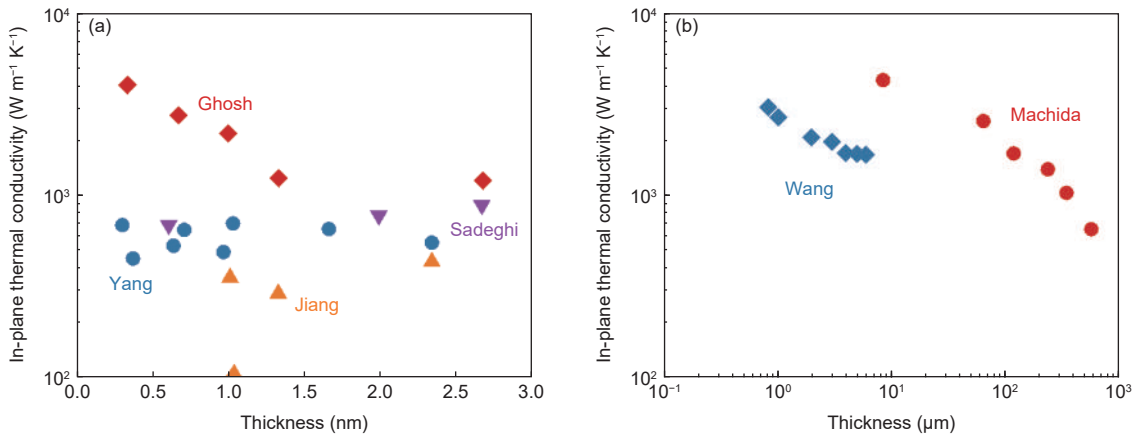

Fig. 11 Thickness-dependent in-plane thermal conductivity of graphite at room temperature: (a) Thickness of several layers[30–33] and (b) thickness within the range of several micrometers to bulk graphite[35, 36]. Reprinted with permission.

of the MFP along the c-axis. Zheng et al.[48] used TDTR to measure the thermal conductivity of CVD graphite thin-films with various thicknesses (20-140 nm) grown on a single-crystal Ni (111) substrate. The obtained $\Lambda_{\perp}$ of 3.3 $Wm^{-1}K^{-1}$ is still lower than that of bulk graphite, indicating that the MFP in the cross direction is larger than 140 nm. Fu et al.[49] measured the $\Lambda_{\perp}$ of graphite with thicknesses of 24-714 nm at room temperature and found an increase in $\Lambda_{\perp}$ with increasing thickness without saturation, which means that the cross-plane MPF of graphite can be larger than 700 nm. Zhang et al.[50] further measured $\Lambda_{\perp}$ of graphite flakes with thicknesses of 24 nm to 21.9 μm. At 300 K, $\Lambda_{\perp}$ saturated at a thickness of approximately 800 nm, indicating that the MFP was at least several hundred nanometers thick. The experiment results obtained by Fu et al.[48] and Zhang et al.[49] are shown in Fig. 12.

4.5 Applications of graphite in thermal management

Because of their extremely high thermal conductivities, graphite and its composites are considered to be the most promising thermal management materials. Yan et al.[3] first transferred few-layer graphene exfoliated from HOPG on top of an AlGaN/GaN transistor. The temperatures of the hotspots can be lowered by approximately 20 °C at an operating power of 13 W mm^{-1}, and the device lifetime can be increased by an order of magnitude[3]. Peng et al.[51] reported ultrahigh thermal conductive (1 940 ± 113 $Wm^{-1}K^{-1}$) and super flexible graphene films obtained by folding atomically thin graphene into microfolds. In addition, Wang et al.[52] fabricated centimeter-scale crystalline films with a high thermal conductivity of 2 292 ± 159 $Wm^{-1}K^{-1}$ by stacking 100 layers of CVD-grown graphene. For practical applications, graphite thin films graphitized from assembled graphene oxide flakes or pyrolytic graphite sheets from polyimide have been developed as new heat-dissipation materials. The thermal conductivities of these films vary widely, from several hundreds to 2 025 $Wm^{-1}K^{-1}$. This scattering property results from the difference in the structural defects, functional groups, grain size, and orientation of the graphite crystallites[53–58].

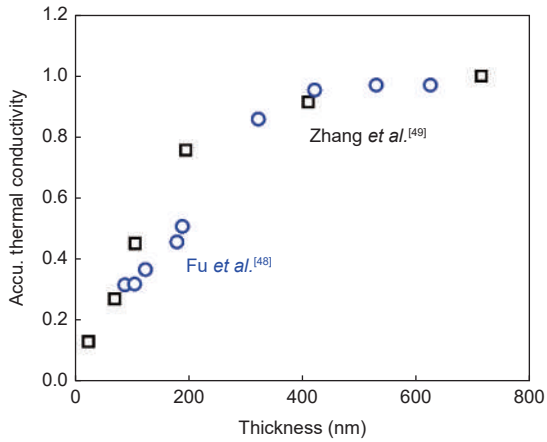

Fig. 12　Room-temperature cross-plane phonon MFPs of graphite measured by Fu et al.[49] and Zhang et al.[50]. Reprinted with permission.

5　Conclusions

This paper reviewed the theoretical and experimental results of the CTE and thermal conductivity of graphite and will pave the way for future research. However, several issues regarding the thermal properties of graphite still need to be clarified, including (1) modeling the change in the CTE of polycrystalline graphite under neutron irradiation, (2) the measurement of nanoscale thermal transport with graphite crystals, (3) the accurate determination of the MFP of graphite, (4) the thermal characterization of graphite materials under extreme conditions. The solutions to these problems will depend on the establishment of more advanced thermal measurement technologies and experiment conditions.

Acknowledgements

This study was supported by the National Natural Science Foundation of China (51872083).

References

[1] Moore A L, Shi L. Emerging challenges and materials for thermal management of electronics[J]. Materials Today, 2014, 17: 163-174.

[2] Pop E. Energy dissipation and transport in nanoscale devices[J]. Nano Research, 2010, 3: 147-169.

[3] Yan Z, Liu G, Khan J M, et al. Graphene quilts for thermal management of high-power GaN transistors[J]. Nature Communications, 2012, 3: 1-8.

[4] Edwards I, Marsh H, Menendez R. Introduction to Carbon Science

[M]. Butterworth-Heinemann, 1989.
[5] Xu X, Pereira L, Wang Y, et al. Length-dependent thermal conductivity in suspended single-layer graphene[J]. Nature Communications, 2014, 5: 3689.
[6] Lee S, Broido D, Esfarjani K, et al. Hydrodynamic phonon transport in suspended graphene[J]. Nature Communications, 2015, 6: 6290.
[7] Cepellotti A, Fugallo G, Paulatto L, et al. Phonon hydrodynamics in two-dimensional materials[J]. Nature Communications, 2015, 6: 6400.
[8] Feng T, Ruan X. Four-phonon scattering reduces intrinsic thermal conductivity of graphene and the contributions from flexural phonons[J]. Physical Review B, 2018, 97: 045202.
[9] Gu X, Fan Z, Bao H, et al. Revisiting phonon-phonon scattering in single-layer graphene[J]. Physical Review B, 2019, 100: 064306.
[10] Nelson J B, Riley D P. The thermal expansion of graphite from 15 °C to 800 °C: Part II. Theoretical[J]. Proceedings of the Physical Society (1926-1948), 1945, 57(6): 486.
[11] Steward E G, Cook B P. X-ray measurement of thermal expansion perpendicular to the layer planes of artificial and natural graphites[J]. Nature, 1960, 185: 78-80.
[12] Harrison J W. Absolute measurements of the coefficient of thermal expansion of pyrolytic graphite from room temperature to 1200 K and a comparison with current theory[J]. High temperatures-High Pressures, 1977, 9: 211-229.
[13] Morgan W C. Thermal expansion coefficients of graphite crystals[J]. Carbon, 1972, 10: 73-79.
[14] Riley D P. The thermal expansion of graphite: part II. Theoretical[J]. Proceedings of the Physical Society (1926-1948), 2002, 57: 486.
[15] Tsang D K, Marsden B J, Fok S L, et al. Graphite thermal expansion relationship for different temperature ranges[J]. Carbon, 2005, 43: 2902-2906.
[16] Mounet N, Marzari N. First-principles determination of the structural, vibrational and thermodynamic properties of diamond, graphite, and derivatives[J]. Physical Review B, 2005, 71: 205214.
[17] Boi F S, Liu M, Xia J, et al. Temperature driven anomalous unit-cell c-axis shifts in highly oriented pyrolytic graphite measured at the magic-angle[J]. Carbon, 2019, 145: 690-693.
[18] Kellett E A, Richards B P. The thermal expansion of graphite within the layer planes[J]. Journal of Nuclear Materials, 1964, 12: 184-192.
[19] Akikubo K, Kurahashi T, Kawaguchi S, et al. Thermal expansion measurements of nano-graphite using high-temperature X-ray diffraction[J]. Carbon, 2020, 169: 307-311.
[20] Mag-isa A E, Kim J, Oh C. Measurements of the in-plane coefficient of thermal expansion of freestanding single-crystal natural graphite[J]. Materials Letters, 2016, 171: 312-314.
[21] Weast Robert C. CRC Handbook of Chemistry and Physics [M]. CRC handbook of chemistry and physics, 1988.
[22] Ho C Y, Powell R W, Liley P E. Thermal conductivity of the elements[J]. Journal of Physical and Chemical Reference Data, 1972, 1: 279-421.
[23] Touloukian Y S, Powell R W, Ho C Y, et al. (Thermophysical and Electronic Properties Information Analysis Center, 1971).
[24] Taylor R. The thermal conductivity of pyrolytic graphite[J]. Philosophical Magazine, 1966, 13: 157-166.
[25] Nihira T, Iwata T. Thermal resistivity changes in electron-irradiated pyrolytic graphite[J]. Japanese Journal of Applied Physics, 1975, 14: 1099.
[26] Schmidt A J. Massachusetts Institute of Technology [M]. 2008.
[27] Feser J P, Cahill D G. Probing anisotropic heat transport using time-domain thermoreflectance with offset laser spots[J]. Review of Scientific Instruments, 2012, 83: 104901.
[28] Jiang P, Qian X, Yang R. Time-domain thermoreflectance (TDTR) measurements of anisotropic thermal conductivity using a variable spot size approach[J]. Review of Scientific Instruments, 2017, 88: 074901.
[29] Qian X, Ding Z, Shin J, et al. Accurate measurement of in-plane thermal conductivity of layered materials without metal film transducer using frequency domain thermoreflectance[J]. Review of Scientific Instruments, 2020, 91: 064903.
[30] Taylor R, Gilchrist K E, Poston, L J. Thermal conductivity of polycrystalline graphite[J]. Carbon, 1968, 6: 537-544.
[31] Taylor R, Kelly B T, Gilchrist K E. The thermal conductivity of fast neutron irradiated graphite[J]. Journal of Physics and Chemistry of Solids, 1969, 30: 2251-2267.
[32] Maruyama T, Harayama M. Neutron irradiation effect on the thermal conductivity and dimensional change of graphite materials[J]. Journal of Nuclear Materials, 1992, 195: 44-50.
[33] Hooker C N, Ubbelohde A R, Young D A. Anisotropy of thermal conductance in near-ideal graphite[J]. Proceedings of the Royal Society of London. Series A, Mathematical and physical sciences, 1965, 284: 17-31.
[34] Slack G A. Anisotropic thermal conductivity of pyrolytic graphite[J]. Physical Review, 1962, 127: 694-701.
[35] Issi J, Heremans J, Dresselhaus M S. Electronic and lattice contributions to the thermal conductivity of graphite intercalation compounds[J]. Physical Review B, 1983, 27: 1333.
[36] Boxus J, Poulaert B, Issi J P, et al. Low temperature thermal conductivity of graphite-$FeCl_3$ intercalation compounds[J]. Solid State Communications, 1981, 38: 1117-1119.
[37] Ghosh S, Bao W, Nika D L, et al. Dimensional crossover of thermal transport in few-layer graphene[J]. Nature materials, 2010, 9: 555-558.
[38] Sadeghi M M, Jo I, Shi L. Phonon-interface scattering in multilayer graphene on an amorphous support[J]. Proceedings of the National Academy of Sciences, 2013, 110: 16321-16326.
[39] Jang W, Chen Z, Bao W, et al. Thickness-dependent thermal conductivity of encased graphene and ultrathin graphite[J]. Nano Letters, 2010, 10: 3909-3913.
[40] Seol J H, Jo I, Moore A L, et al. Two-dimensional phonon transport in supported graphene[J]. Science, 2010, 328: 213-216.
[41] Lindsay L, Broido D A, Mingo N. Flexural phonons and thermal transport in graphene[J]. Physical Review B, 2010, 82: 115427.

[42] Machida Y, Matsumoto N, Isono T, et al. Phonon hydrodynamics and ultrahigh-room-temperature thermal conductivity in thin graphite[J]. Science, 2020, 367: 309-312.

[43] Wang N, Samani M K, Li H, et al. Tailoring the thermal and mechanical properties of graphene film by structural engineering[J]. Small, 2018, 14: 1801346.

[44] Murakami M, Nishiki N, Nakamura K, et al. High-quality and highly oriented graphite block from polycondensation polymer films[J]. Carbon, 1992, 30: 255-262.

[45] Fugallo G, Cepellotti A, Paulatto L, et al. Thermal conductivity of graphene and graphite: Collective excitations and mean free paths[J]. Nano Letters, 2014, 14: 6109-6114.

[46] Wei Z, Yang J, Chen W, et al. Phonon mean free path of graphite along the c-axis[J]. Applied Physics Letters, 2014, 104: 081903.

[47] Harb M, von Korff Schmising C, Enquist H, et al. The c-axis thermal conductivity of graphite film of nanometer thickness measured by time resolved X-ray diffraction[J]. Applied Physics Letters, 2012, 101: 233108.

[48] Zheng Q, Braun P V, Cahill D G. Thermal conductivity of graphite thin films grown by low temperature chemical vapor deposition on Ni (111)[J]. Advanced Materials Interfaces, 2016, 3: 1600234.

[49] Fu Q, Yang J, Chen Y, et al. Experimental evidence of very long intrinsic phonon mean free path along the c-axis of graphite[J]. Applied Physics Letters, 2015, 106: 031905.

[50] Zhang H, Chen X, Jho Y, et al. Temperature-dependent mean free path spectra of thermal phonons along the c-axis of graphite[J]. Nano Letters, 2016, 16: 1643-1649.

[51] Peng L, Xu Z, Liu Z, et al. Ultrahigh Thermal conductive yet superflexible graphene films[J]. Advanced Materials, 2017, 29: 1700589.

[52] Wang B, Cunning B V, Kim N Y, et al. Ultrastiff, strong, and highly thermally conductive crystalline graphitic films with mixed stacking order[J]. Advanced Materials, 2019, 31: 1903039.

[53] Akbari A, Cunning B V, Joshi S R, et al. Highly Ordered and dense thermally conductive graphitic films from a graphene oxide/reduced graphene oxide mixture[J]. Matter, 2020, 2: 1198-1206.

[54] Xin G, Sun H, Hu T, et al. Large-area freestanding graphene paper for superior thermal management[J]. Advanced Materials, 2014, 26: 4521-4526.

[55] Chen S, Wang Q, Zhang M, et al. Scalable production of thick graphene film for next generation thermal management application[J]. Carbon, 2020, 167: 270-277.

[56] Renteria J D, Ramirez S, Malekpour H, et al. Strongly anisotropic thermal conductivity of free-standing reduced graphene oxide films annealed at high temperature[J]. Advanced Functional Materials, 2015, 25: 4664-4672.

[57] Inagaki M, Kaburagi Y, Hishiyama Y. Thermal management material: Graphite[J]. Advanced Engineering Materials, 2014, 16: 494-506.

[58] Shen B, Zhai W, Zheng W. Ultrathin flexible graphene film: An excellent thermal conducting material with efficient EMI shielding[J]. Advanced Functional Materials, 2014, 24: 4542-4548.